Cellular/Molecular

# μ-Opioid Inhibition of $Ca^{2+}$ Currents and Secretion in Isolated Terminals of the Neurohypophysis Occurs via Ryanodine-Sensitive $Ca^{2+}$ Stores

**Cristina Velázquez-Marrero, Sonia Ortiz-Miranda, Héctor G. Marrero, Edward E. Custer, Steven N. Treistman, and José R. Lemos**

Department of Microbiology and Physiological Systems and Program in Neuroscience, University of Massachusetts Medical School, Worcester, Massachusetts 01605

**μ-Opioid agonists have no effect on calcium currents ($I_{Ca}$) in neurohypophysial terminals when recorded using the classic whole-cell patch-clamp configuration. However, μ-opioid receptor (MOR)-mediated inhibition of $I_{Ca}$ is reliably demonstrated using the perforated-patch configuration. This suggests that the MOR-signaling pathway is sensitive to intraterminal dialysis and is therefore mediated by a readily diffusible second messenger. Using the perforated patch-clamp technique and ratio-calcium-imaging methods, we describe a diffusible second messenger pathway stimulated by the MOR that inhibits voltage-gated calcium channels in isolated terminals from the rat neurohypophysis (NH). Our results show a rise in basal intracellular calcium ($[Ca^{2+}]_i$) in response to application of [D-Ala$^2$-N-Me-Phe$^4$,Gly5-ol]-Enkephalin (DAMGO), a MOR agonist, that is blocked by D-Phe-Cys-Tyr-D-Trp-Orn-Thr-Pen-Thr-$NH_2$ (CTOP), a MOR antagonist. Buffering DAMGO-induced changes in $[Ca^{2+}]_i$ with BAPTA-AM completely blocked the inhibition of both $I_{Ca}$ and high-$K^+$-induced rises in $[Ca^{2+}]_i$ due to MOR activation, but had no effect on κ-opioid receptor (KOR)-mediated inhibition. Given the presence of ryanodine-sensitive stores in isolated terminals, we tested 8-bromo-cyclic adenosine diphosphate ribose (8Br-cADPr), a competitive inhibitor of cyclic ADP-ribose (cADPr) signaling that partially relieves DAMGO inhibition of $I_{Ca}$ and completely relieves MOR-mediated inhibition of high-$K^+$-induced and DAMGO-induced rises in $[Ca^{2+}]_i$. Furthermore, antagonist concentrations of ryanodine completely blocked MOR-induced increases in $[Ca^{2+}]_i$ and inhibition of $I_{Ca}$ and high-$K^+$-induced rises in $[Ca^{2+}]_i$ while not affecting KOR-mediated inhibition. Antagonist concentrations of ryanodine also blocked MOR-mediated inhibition of electrically-evoked increases in capacitance. These results strongly suggest that a key diffusible second messenger mediating the MOR-signaling pathway in NH terminals is $[Ca^{2+}]_i$ released by cADPr from ryanodine-sensitive stores.**

*Key words:* **exocytosis; $I_{Ca}$; MOR modulation; NH terminals; RyR**

## Introduction

The μ-opioid receptor (MOR)-mediated inhibition of the hypothalamic neurohypophysial system (HNS) becomes increasingly evident during pregnancy, but is interrupted before parturition, allowing for strong excitation of oxytocin cells that facilitates birth (Russell et al., 1995; Russell et al., 2003). Corelease of dynorphin-A, an endogenous κ-opioid receptor (KOR) agonist, with vasopressin from dendrites facilitates activity-dependent modulation of vasopressinergic neurons (Brown and Bourque, 2004; Brown et al., 2004; Roper et al., 2004; Brown et al., 2006; Sabatier and Leng, 2007). Isolated HNS terminals demonstrate inhibition of release in the presence of either MOR or KOR agonists for both oxytocin and vasopressin (Sumner et al., 1990; Kato et al., 1992; Russell et al., 1993); $I_{Ca}$ is similarly inhibited (Rusin et al., 1997; Ortiz-Miranda et al., 2003; Ortiz-Miranda et al., 2005). The signaling mechanism and modulatory importance of MOR and KOR activation at these presynaptic terminals and subsequent $I_{Ca}$ inhibition, however, is not well understood. Given the level of endogenous opioid modulation in the HNS, this has considerable physiological relevance.

MOR and KOR are G-protein-coupled receptors that could potentially mediate inhibitory effects of opioids/opiates on $I_{Ca}$ through either a membrane-delimited or diffusible second messenger pathway (Wilding et al., 1995; Soldo and Moises, 1998; Kaneko et al., 1998; Connor and Christie, 1999; Chen et al., 2000). The MOR-signaling pathway seems to contrast sharply with that documented for the KOR in the same isolated neurohypophysis (NH) terminals (Velázquez-Marrero et al., 2010).

Received April 23, 2013; revised Jan. 22, 2014; accepted Jan. 25, 2014.

Author contributions: C.V.-M. and J.R.L. designed research; C.V.-M., S.O.-M., and H.G.M. performed research; S.N.T. contributed unpublished reagents/analytic tools; C.V.-M., S.O.-M., H.G.M., and E.E.C. analyzed data; C.V.-M., S.N.T., and J.R.L. wrote the paper.

This work was supported by the National Institutes of Health (Grants R01 NS29470, R21 NS063192, and R01DA10487 to J.R.L.) and the University of Massachusetts Faculty Diversity Scholars Program (Grant P60037094900000 to S.O.-M.).

The authors declare no competing financial interests.

Correspondence should be addressed to José R. Lemos, PhD, Department of Microbiology and Physiological Systems and Program in Neuroscience, University of Massachusetts Medical School, 368 Plantation Street, Worcester, MA 01605. E-mail: Jose.Lemos@umassmed.edu.

Present address of C. Velázquez-Marrero, Héctor G. Marrero, and Steven N. Treistman: Instituto de Neurobiología, 201 Blvd. del Valle, San Juan, Puerto Rico 00901.

DOI:10.1523/JNEUROSCI.2505-13.2014

 0270-6474/14/343733-10$15.00/0

MOR agonists did not inhibit $I_{Ca}$ when recorded using the whole-cell patch-clamp configuration, in contrast to KOR-mediated inhibition (Rusin et al., 1997). However, MOR-mediated inhibition of $I_{Ca}$ is demonstrated using the perforated-patch configuration of the patch-clamp method (Ortiz-Miranda et al., 2005). This strongly suggests that the MOR-signaling pathway at the NH terminals is sensitive to intraterminal dialysis and is therefore mediated by a readily diffusible second messenger. Furthermore, unlike the KOR-mediated inhibition of $I_{Ca}$, MOR inhibition is not relieved by a strong depolarizing prepulse (Velázquez-Marrero et al., 2010).

Ryanodine-sensitive calcium stores have been shown to be targets of G-protein opioid activation (Tai et al., 1992; Hauser et al., 1996; Samways and Henderson, 2006). In isolated HNS terminals, we have characterized ryanodine- and voltage-sensitive $[Ca^{2+}]_i$ release events, known as syntillas (De Crescenzo et al., 2004). Furthermore, the cyclic ADP-ribose (cADPr) signaling pathway initiates a signaling cascade leading to activation of the ryanodine receptor *in vivo* and subsequent release of $[Ca^{2+}]_i$ from ryanodine-sensitive stores (Galione, 1994; Sitsapesan et al., 1995; Morita et al., 2002). Interestingly, recent studies have shown the cADPr signaling pathway has a significant role in oxytocin (OT) release from isolated HNS terminals (Higashida et al., 2007; Jin et al., 2007). We propose that, in HNS terminals, activation of the MOR triggers a rise in intraterminal basal calcium released from ryanodine-sensitive stores via activation of the cADPr signaling cascade. This rise in $[Ca^{2+}]_i$ could lead to calcium-dependent inhibition of $I_{Ca}$ and subsequent inhibition of depolarization-induced neuropeptide release.

## Materials and Methods

*Isolation of nerve endings.* Male Sprague Dawley rats (Taconic Farms) weighing 200–250 g were sedated using $CO_2$ and immediately decapitated. The pituitary gland was isolated as described previously (Lemos et al., 1986; Knott et al., 2005). Briefly, after removal of the anterior and intermediate lobes, the posterior pituitary was homogenized in 270 $\mu$l of buffer at 37°C containing the following (in mM): 270 sucrose, 0.004 EGTA, and 10 HEPES-Tris buffered at pH 7.25, 298–302 mOsmol/L. The solution containing the homogenate was plated on a 35 mm Petri dish and carefully washed in low-calcium Locke's solution consisting of modified normal Locke's (NL) containing the following (in mM): 145 NaCl, 2.5 KCl, 10 HEPES, 1.2 glucose, 0.8 $CaCl_2$, and 0.4 $MgCl_2$, pH 7.4, 298–302 mOsmol/L.

*Electrophysiological experiments.* The NH was isolated and homogenized as described previously (Brethes et al., 1987; Brown et al., 2006). Current recordings were obtained using the perforated-patch configuration on isolated HNS terminals. Using an inverted microscope, the terminals were identified visually by their characteristic appearance, spherical shape, lack of nuclei, and size (5–10 $\mu$m in diameter). The pipette solution consisted of the following (in mM): 145 Cs-gluconate, 15 CsCl, 2 $MgCl_2$, 2 NaCl, 7 glucose, and 10 HEPES, pH 7.3, 295 mOsm. Amphotericin B at a concentration of 30 $\mu$M (Sigma) was added as a perforating agent. The bath solution consisted of the following (in mM): 145 NaCl, 5 KCl, 1 $MgCl_2$, 10 HEPES, 10 glucose, 1.2 $CaCl_2$, pH 7.5, in NL. In all experiments, TTX (100 nM) was added to the bath to block sodium influx via voltage-gated sodium channels. The pipette resistance was 5–8 M$\Omega$. Pipettes were made of thin borosilicate glass (Drummond Scientific). After perforation, the terminals were voltage clamped at −80 mV. Depolarization was applied every 30 s to 0 mV for 250–300 ms. The preparation was either continually perfused via a gravity-driven perfusion or was left in a static, nonperfused bath (as noted). Agonists and antagonists were either applied through the gravity-driven perfusion system or added to the static bath. All experiments were performed at room temperature (25°C). Data were acquired, stored, and analyzed using a Pentium I computer (Gateway) and pClamp 7 software (Molecular Devices). Currents were corrected online using an inverted P/4 protocol. Inactivation time constants ($\tau$) were obtained from single exponential fits (Igor; Wavemetrics or PClamp6) on inward $I_{Ca}$ for 5 ms after peak current and 3 ms before the end of stimulus.

*Calcium imaging.* Freshly dissociated nerve terminals (Nordmann et al., 1987) prepared from adult Sprague Dawley CD rats were incubated with 2.5 $\mu$M Fura-2 AM for 45 min at 37°C and thoroughly washed with NL solution containing the following (in mM): 145 NaCl, 5 KCl, 10 HEPES, 10 glucose, 1 $MgCl_2$, and 2.2 $CaCl_2$, pH 7.4. $Ca^{2+}$ free bath solution contained the following (in mM): 145 NaCl, 5 KCl, 10 HEPES, 10 glucose, 0.0002 EGTA, and 1 $MgCl_2$, pH 7.4, and gave a calculated free $[Ca^{2+}]$ of zero. Cytosolic $[Ca^{2+}]$ was determined with ratiometric indicator Fura-2 AM-loaded terminals. Calibration of Fura-2 was done both *in vitro* using the Invitrogen Calcium Calibration Buffer Kit (catalog #F-6774) and *in situ* using predetermined $[Ca^{2+}]_{free}$ buffered solutions on terminals loaded with Fura-2 AM and using the Br-A23187 divalent cation ionophore. The $K_d$ was calculated from a plot generated by scanning the ratio of the emission at the two corresponding wavelengths against $[Ca^{2+}]_{free}$ across the zero to saturating $[Ca^{2+}]_{free}$ concentrations. The results were plotted as a double log of the calcium response resulted in a straight line, with the *x*-intercept being equal to the log of the apparent $K_d$ indicator, which was determined under *in situ* conditions to be ~200 nM across the physiologically relevant concentration rage of 0–35 $\mu$M $[Ca^{2+}]_{free}$. The calculations were performed as described previously (Grynkiewicz et al., 1985). Resting values for global cytosolic $[Ca^{2+}]$ in the presence and absence of extracellular $Ca^{2+}$ were 73.3 ± 6.9 nM ($n$ = 12) and 46.2 ± 7.5 nM ($n$ = 8), respectively, and these values demonstrated a statistically significant difference. In all cases, changes in $[Ca^{2+}]_i$ were determined by measuring total calcium.

Fluorescence images using Fura-2 AM as a calcium indicator were viewed with a Nikon Diaphot TMD microscope using a Zeiss Plan-NEOFLUAR 100× oil-immersion lens and fitted with a Photometrics SenSys CCD camera. The camera was interfaced to the inverted microscope adapted with a Chroma 71000A Fura2 filter cube. The terminals were excited using a Xenon arc lamp within a Lambda DG4 high-speed filter changer (Sutter Instruments) with the appropriate filters (340 and 380 nm wavelengths). Intraterminal emission of Fura-2 $Ca^{2+}$ indicator was gathered at 510 nm wavelength. Fluorescent images were acquired and processed with Axon Imaging Workbench 2.1 software (Molecular Devices).

*Capacitance measurements.* Freshly dissociated terminals (Nordmann et al., 1987) from adult Sprague Dawley CD rats weighing 200–250 g were plated in NL solution with 1.2 mM $CaCl_2$. Tight seal "whole terminal" recordings were obtained using the perforated-patch configuration described in Electrophysiological experiments, above. The pipette resistances ranged from 5 to 8 M$\Omega$. Perforation of the terminals' membrane was obtained by adding 30 $\mu$M amphotericin B (Sigma) to the pipette solution containing the following (in mM): 145 Cs-gluconate, 15 CsCl, 5 NaCl, 2 $MgCl_2$, 7 glucose, and 10 HEPES pH 7.3. The bath solution contained the following (in mM): 145 NaCl, 5 KCl, 1 $MgCl_2$, 10 HEPES, 10 glucose, and 1.2 $CaCl_2$ or 0.2 EGTA, pH 7.5. Capacitance measurements were obtained using the piecewise linear method (Knott et al., 2007). The changes in capacitance induced by a depolarizing pulse (750 ms duration) were measured 1 s after cessation of stimulus to avoid interference of stimulus "end-tail" effects. These stimulus-induced capacitance changes were measured for isolated terminals (perforated-patch) using the piecewise method (Neher and Marty, 1982; Lindau and Neher, 1988; Gillis, 1995). Briefly, the method consists of applying a sinusoidal voltage of low amplitude to the sample (to avoid voltage-elicited channel currents) and obtaining the phase shift of the resultant sinusoidal current. Changes in this phase shift ("locked-in") are used in a formula (computer software that emulates a lock-in amplifier) for the determination of the capacitance changes (i.e., the capacitance that would cause such change of phase shift). The method is sensitive to very small changes in capacitance and, in practice, large baseline capacitance and resistance (series) transients must be compensated (i.e., null) before measuring any small capacitance change. In this particular case, the parameters used were a sine wave of 1000 Hz at ±25 mV (approximately the holding potential), with the program reporting a

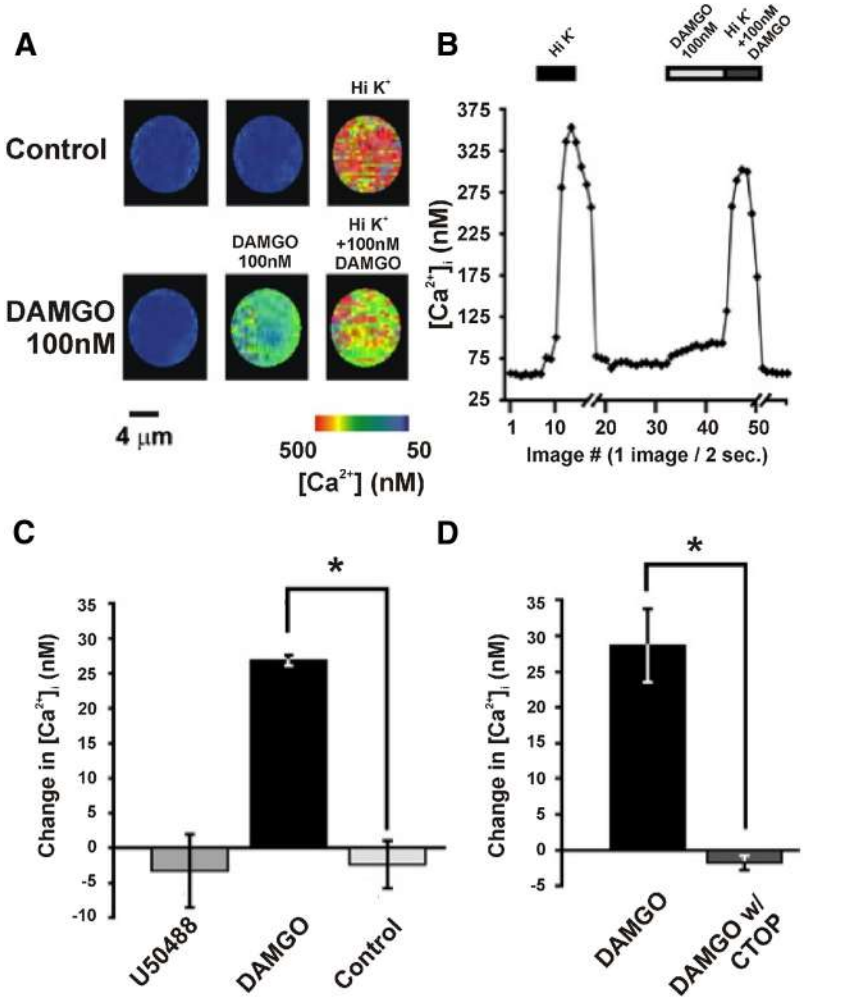


**Figure 1.** MOR but not KOR agonists trigger a rise in basal $[Ca^{2+}]_i$ preceding MOR-mediated inhibition of high-$K^+$-induced rise in $[Ca^{2+}]_i$. ***A***, Images of a Fura-2 AM-loaded single terminal ~10 s apart challenged with high-$K^+$ ($HiK^+$) in 2.2 mM $[Ca^{2+}]_o$ for 5 s with and without 100 nM DAMGO preexposure. ***B***, Plot of changes in $[Ca^{2+}]_i$ over time of a different single isolated HNS terminal loaded with Fura 2-AM: high $K^+$ (as labeled) exposures for 5 s and DAMGO (as labeled) pretreatment for 10 s followed by high $K^+$ in the presence of 100 nM DAMGO (as labeled). Double forward slashes in *x*-axis represent 30 s breaks in image acquisition to allow recovery from high $K^+$ treatment. ***C***, $[Ca^{2+}]_i$ change from baseline in response to 100 nM U50488, 100 nM DAMGO, and control treatment containing modified NL without $Ca^{2+}$ (as labeled); $n = 5$ terminals. ***D***, Rise in $[Ca^{2+}]_i$ due to 100 nM DAMGO application is blocked in the presence of 100 nM CTOP (as labeled); $n = 4$ terminals. Asterisks (*) represent statistical differences ($p = 0.002$).

capacitance averaged for every 30 points (24 $\mu$s sampling rate). The current was filtered at a bandwidth of 5000 Hz.

*Statistical comparisons*. In all cases, data are reported as mean ± SEM; *n* indicates the number of terminals. Statistical analysis was performed using either a Student's *t* test or a one-way ANOVA followed by a Dunnett's posttest. The criterion for significance in all cases was $p < 0.05$.

## Results

### MOR but not KOR agonist elicits a rise in basal intraterminal $[Ca^{2+}]$

To determine whether intraterminal $Ca^{2+}$ ($[Ca^{2+}]_i$) was part of a diffusible second messenger pathway mediating opioid receptor signaling in isolated HNS terminals, we monitored it in response to both MOR and KOR activation. Fura-2 AM ratio calcium imaging of isolated HNS terminals showed a significant inhibition of high-$K^+$-induced rises in $[Ca^{2+}]_i$ when treated with either MOR agonists (Fig. 1*A*,*B*) or KOR agonists (Fig. 2*C*). Furthermore, pretreatment with 100 nM DAMGO (a MOR agonist) alone at either 2.2 (Fig. 1*A*,*B*) or 0 mM (Fig. 1*C*,*D*) external calcium ($[Ca^{2+}]_o$) elicited a rise in basal $[Ca^{2+}]_i$. This did not occur when terminals were pretreated with 100 nM U50488 (a KOR agonist) or puffed with control 0 mM $[Ca^{2+}]_o$ NL (Fig. 1*C*). Application of the MOR antagonist CTOP (Fig. 1*D*) blocked the DAMGO-induced rise in basal $[Ca^{2+}]_i$. Changes in basal intraterminal calcium concentration were 26.9 ± 0.8 nM by 100 nM DAMGO in 2.2 mM $[Ca^{2+}]_o$ NL and (28.7 ± 5.1 nM) in 0 mM $[Ca^{2+}]_o$ with 100 nM DAMGO. Differences in $[Ca^{2+}]_i$ were −3.3 ± 5.2 nM due to 100 nM U50488, control was −2.4 ± 3.4 nM, and 100 nM DAMGO in the presence of CTOP was −1.8 ± 1.0 nM (all in 0 mM $[Ca^{2+}]_o$). Control applications (Fig. 1*C*) caused an artifactual drop in $[Ca^{2+}]_i$, which may be an inherent factor in all treatment applications and could therefore lead to an underestimation of the DAMGO-induced rise in $[Ca^{2+}]_i$. Control baseline $[Ca^{2+}]_i$ averaged 71.6 ± 15.7 nM.

### MOR- but not KOR- mediated inhibition is blocked by intraterminal calcium buffering

To determine whether the rise in $[Ca^{2+}]_i$ due to MOR agonist application is essential for subsequent inhibition of $I_{Ca}$, we partially buffered $[Ca^{2+}]_i$ using BAPTA-AM and monitored the effects on both $I_{Ca}$ and high-$K^+$-induced rises in $[Ca^{2+}]_i$. Empirically determined incubation periods of 5–10 min using low concentrations (10 $\mu$M) of BAPTA-AM were followed by a brief wash. Using this procedure, BAPTA-AM buffered DAMGO-induced rises in intraterminal calcium from 22.7 ± 2.4 nM down to 0.2 ± 0.5 nM (Fig. 2*A*). However, this concentration of BAPTA-AM did not block total high-$K^+$-induced rise in $[Ca^{2+}]_i$ (Fig. 2*B*,*C*). Effects on both high-$K^+$-induced rises in $[Ca^{2+}]_i$ and $I_{Ca}$ were measured for both MOR- and KOR-mediated inhibitions using the same concentration of BAPTA-AM for identical incubation periods. All measurements were made as either changes in basal $[Ca^{2+}]_i$ or as a percentage of control. Control measurements were under identical conditions without opioid/opiate treatments. High-$K^+$-induced rises in $[Ca^{2+}]_i$ in the presence of 100 nM DAMGO were 54.1 ± 3.4% of control responses. High $K^+$ in the presence of 100 nM U50488 was also inhibited to 70.9 ± 2.8% of controls (Fig. 2*C*). However, after incubation with 10 $\mu$M BAPTA-AM, terminals exposed to 100 nM DAMGO showed no significant inhibition (109.9 ± 12.8%) of the high-$K^+$-induced rise in $[Ca^{2+}]_i$ ($p = 0.05$), as opposed to without BAPTA-AM treatment ($p = 0.002$). In contrast, inhibition (78.5 ± 2.8%) of the high $K^+$ response by 100 nM U50488 remained the same with versus without BAPTA-AM treatment ($p = 0.3$). Baseline $[Ca^{2+}]_i$ before high $K^+$ was not statistically different ($p = 0.16$) with (77.9 ± 12.8 nM) versus without (86.5 ± 27.5 nM) 5 min preincubation by 10 $\mu$M BAPTA-AM. Total $[Ca^{2+}]_i$ was not significantly changed (see legend to Fig. 2). Furthermore, *m*M

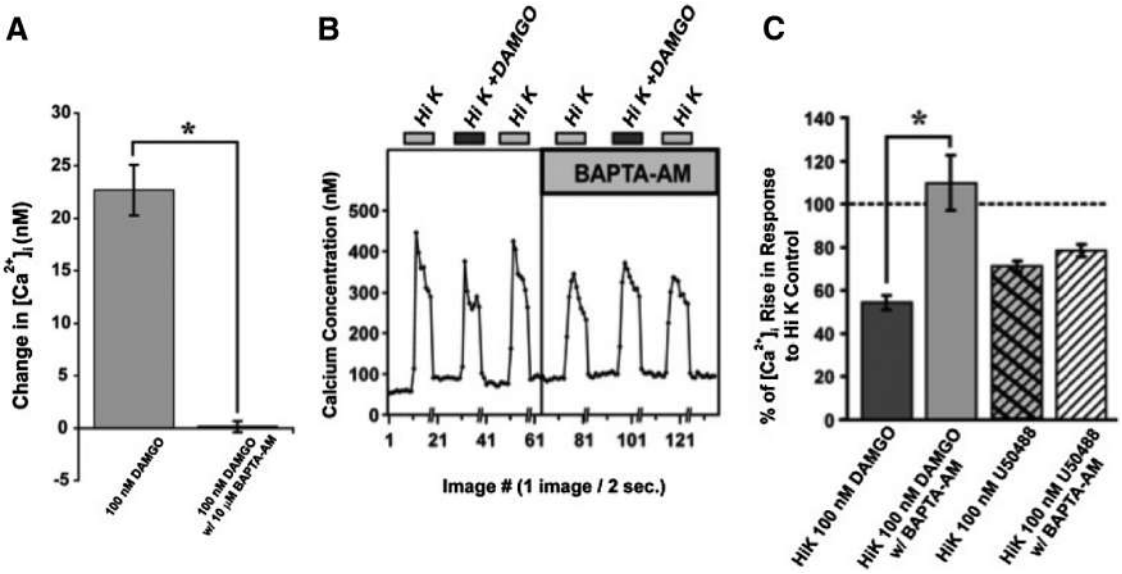


**Figure 2.** BAPTA-AM relieves rise in basal $[Ca^{2+}]_i$ due to MOR agonist and MOR- but not KOR-mediated inhibition of high-$K^+$-induced rise in $[Ca^{2+}]_i$. ***A***, Bar graph of absolute change in $[Ca^{2+}]_i$ from baseline in the presence of 100 nM DAMGO with and without a 5 min preincubation with 10 $\mu$M BAPTA-AM, in 2.2 mM $[Ca^{2+}]_o$. Preincubation with BAPTA-AM completely blocks the rise in basal $[Ca^{2+}]_i$ due to $\mu$-opioid agonist. Asterisk (*) represents statistical difference ($p = 0.004$) between 100 nM DAMGO and 100 nM DAMGO pretreated with 10 $\mu$M BAPTA-AM ($n = 3$). ***B***, Plot of changes in $[Ca^{2+}]_i$ of a single HNS terminal loaded with Fura-2 AM with and without a brief 10 $\mu$M BAPTA-AM preincubation treated with high $K^+$ ($HiK^+$) or high $K^+$ with 100 nM DAMGO (premixed for a simultaneous exposure) in NL solution. Double forward slashes in *x*-axis represent 30 s breaks in image acquisition to allow high $K^+$ treatment to recover. ***C***, Bar graph quantifying changes in $[Ca^{2+}]_i$ in response to high K, and high $K^+$ with 100 nM DAMGO or 100 nM U50488 with and without BAPTA-AM preincubation ($n = 4$). Asterisk (*) represents statistically significant differences ($p \leq 0.001$). Total $[Ca^{2+}]_i$ rise due to high $K^+$ are not significantly ($p > 0.05$) changed with BAPTA, probably because mM BAPTA is needed to block the high $K^+$ response (Stuenkel and Nordmann, 1993).

BAPTA is needed to affect high $K^+$ peaks in $[Ca^{2+}]_i$. Therefore, changes in responses to opioids cannot be attributed to initial differences in baseline $[Ca^{2+}]_i$.

### Effects on calcium currents

Buffering $[Ca^{2+}]_i$ also blocked inhibition of $I_{Ca}$ by MOR but not KOR agonists. Terminals treated with 100 nM DAMGO were 82.2 ± 4.0% of control currents and were 88.7 ± 2.3% with 100 nM U50488 (Fig. 3). After preincubation with 10 $\mu$M BAPTA-AM, 100 nM DAMGO elicited no inhibition, with $I_{Ca}$ being 98.9 ± 1.2% of control. Exposing BAPTA-AM-treated terminals to 100 nM U50488 again showed no change in KOR-mediated inhibition, with $I_{Ca}$ remaining at 78.8 ± 4.9% of controls. Statistical analysis determined no significant difference ($p = 0.09$) between terminals treated with 100 nM U50488, with versus without BAPTA-AM preincubation (Fig. 3*C*). There was, however, a statistically significant difference ($p = 0.001$) between terminals treated with 100 nM DAMGO with versus without BAPTA-AM preincubation.

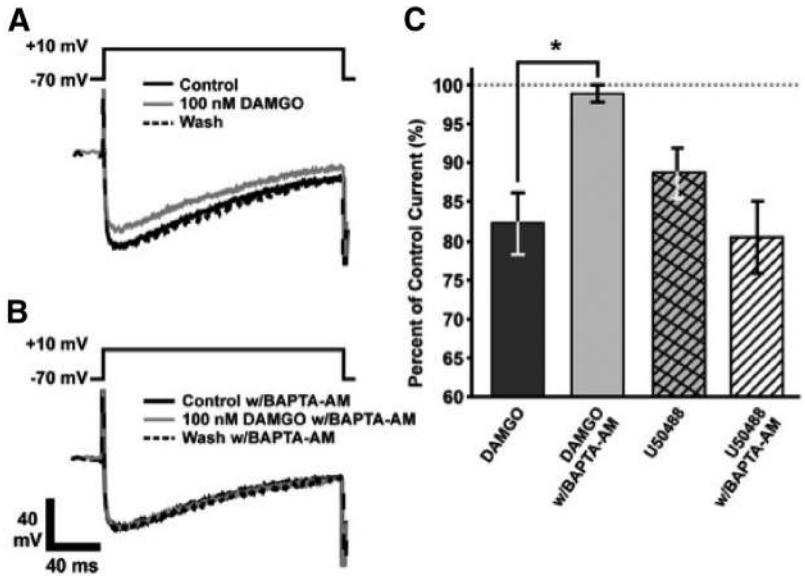


**Figure 3.** BAPTA-AM preincubation relieves MOR- but not KOR-mediated inhibition of calcium currents. ***A***, Representative barium currents of an isolated HNS terminal; control currents (black), 100 nM DAMGO (gray), and wash (dashed-black). ***B***, The same isolated HNS terminal: control is preincubated in 10 $\mu$M BAPTA-AM (black) compared with trace preincubated in BAPTA-AM with 100 nM DAMGO (gray) and wash (dashed-black). ***C***, Bar graph quantifying peak barium currents ($n = 4$) as percentage of control current without any opioid treatment (as labeled). Asterisk (*) represents statistically significant differences ($p = 0.001$).

### cADPr pathway

Because activation of the MOR-induced rise in $[Ca^{2+}]_i$ appears to be essential in mediating MOR inhibition, we investigated whether cADPr was part of this receptor's intraterminal signaling pathway. We examined the effects of the membrane-permeant cADPr antagonist 8-bromo-cyclic adenosine diphosphate ribose (8Br-cADPr) on MOR-mediated inhibition of both high-$K^+$-induced rises in $[Ca^{2+}]_i$ (Fig. 4*A*,*B*) and $I_{Ca}$ (Fig. 4*C*,*D*). Control high-$K^+$-induced changes in $[Ca^{2+}]_i$ were 457.1 ± 13.5 nM, but in the presence of 100 nM DAMGO high-$K^+$-induced changes in $[Ca^{2+}]_i$ decreased to 392.7 ± 19.6 nM ($p = 0.04$). After incubation with 100 nM 8Br-cADPr, terminals exposed to 100 nM

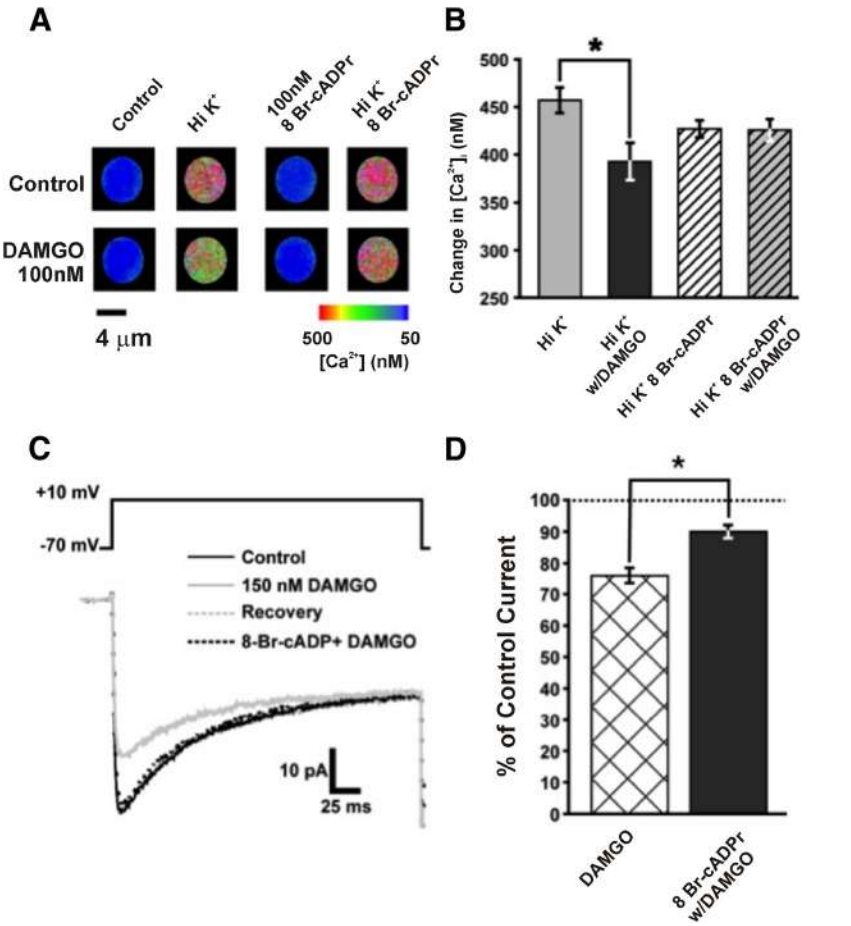


**Figure 4.** cADPr antagonist relieves MOR-mediated inhibition of high-$K^+$-induced rise in $[Ca^{2+}]_i$ and inhibition of calcium currents. ***A***, Consecutive images of a Fura-2 AM-loaded single HNS terminal ~10 s apart challenged with high $K^+$ ($HiK^+$) in 2.2 mM $[Ca^{2+}]_o$ for 10 s with and without 100 nM DAMGO and with and without pretreatment with 100 nM 8Br-cADPr. ***B***, Bar graph summarizing the absolute changes in $[Ca^{2+}]_i$ from baseline in response to high $K^+$ challenges with and without 100 nM DAMGO and with and without incubation with 100 nM 8Br-cADPr ($n = 8$ each). ***C***, Representative $I_{Ca}$ of an isolated HNS terminal; control currents (black), 100 nM DAMGO (gray), recovery (dashed-gray), and 150 nM 8Br-cADPr w/100 nM DAMGO (dashed-black). ***D***, Bar graph quantifying the peak $I_{Ca}$ ($n = 6$) as percentage of control current without DAMGO. Calcium currents with 100 nM DAMGO (as labeled) and with 100 nM DAMGO preincubated with 150 nM 8Br-cADPr (as labeled). Asterisk (*) represents statistically significant differences ($p = 0.02$). Interestingly, 8Br-cADPr had no significant ($p > 0.05$) effect on its own.

DAMGO exhibited only a change in $[Ca^{2+}]_i$ of 425.9 ± 11.3 nM in response to high $K^+$, similar to those in 100 nM 8Br-cADPr without DAMGO treatment (427.2 ± 8.9 nM). Statistical analysis determined no significant difference ($p = 0.43$) in high-$K^+$-induced changes in $[Ca^{2+}]_i$ between terminals treated with 100 nM 8Br-cADPr with versus without 100 nM DAMGO treatment (Fig. 4*A*,*B*). However, in terminals not preincubated with 100 nM 8Br-cADPr, there was a statistically significant difference ($p = 0.0004$) in high-$K^+$-induced changes in $[Ca^{2+}]_i$ between terminals treated with versus without 100 nM DAMGO, as was observed previously. Interestingly, basal $[Ca^{2+}]_i$ without 100 nM 8Br-cADPr preincubation was 79.2 ± 4.0 nM; after preincubation with 100 nM 8Br-cADPr, it was 68.9 ± 2.8 nM ($n = 8$) and these baselines were statistically different ($p = 0.02$).

Terminals treated with 100 nM DAMGO resulted in $I_{Ca}$ measuring 76 ± 2.4% of control currents (Fig. 4*C*,*D*). After preincubation with 100 nM 8Br-cADPr, however, 100 nM DAMGO treatments now showed a partial relief of inhibition, with $I_{Ca}$ at 90 ± 2.1% of control. Intraterminal calcium followed a similar trend, with 8Br-cADPr significantly ($p = 0.004$) blocking the DAMGO-induced rise in $[Ca^{2+}]_i$ (Fig. 5*A*), suggesting that the cADPr pathway is involved in MOR signaling.

### MOR effects are blocked by ryanodine receptor antagonist

We next addressed whether the release of $[Ca^{2+}]_i$ due to MOR activation was from ryanodine-sensitive intraterminal stores. The pharmacology of the ryanodine receptor indicates that 10–100 μM concentrations of ryanodine can block ryanodine channel activity (Coronado, Morrissette et al., 1994; Ehrlich, Kaftan et al., 1994). Therefore, we tested the effects of 100 μM ryanodine on DAMGO-induced rises in basal $[Ca^{2+}]_i$ (Fig. 5*A*) and its inhibition of high-$K^+$-induced rises in $[Ca^{2+}]_i$ (Fig. 5*B*,*C*), $I_{Ca}$ (Figs. 6, 7), and electrically induced capacitance changes (Fig. 7).

DAMGO-induced changes in basal $[Ca^{2+}]_i$ were 21.3 ± 3.2 nM, but after preincubation with 100 μM ryanodine (Fig. 5*A*), these were significantly ($p = 0.0002$) reduced to −0.1 ± 0.8 nM. Likewise, DAMGO-induced changes in basal $[Ca^{2+}]_i$ were blocked by 100 nM 8Br-cADPr (Fig. 5*A*).

Control high-$K^+$-induced changes in $[Ca^{2+}]_i$ were 219.9 ± 21.4 nM. In the presence of 100 nM DAMGO, high-$K^+$-induced changes in $[Ca^{2+}]_i$ were 112.7 ± 8 nM, which represents 51% of the control response (Fig. 5*B*,*C*). After incubation with 100 μM ryanodine, terminals exposed to 100 nM DAMGO now showed a change in $[Ca^{2+}]_i$ of 236.8 ± 8.2 nM in response to high $K^+$, similar to controls without DAMGO (209 ± 13.4 nM) in the presence of 100 μM ryanodine. There was no significant difference ($p = 0.11$) in high-$K^+$-induced changes in basal $[Ca^{2+}]_i$ between control terminals in 100 μM ryanodine and those in 100 μM ryanodine treated with 100 nM DAMGO. However, there was a statistically significant difference ($p = 0.01$) in high-$K^+$-induced changes in $[Ca^{2+}]_i$ between terminals treated with versus without 100 nM DAMGO, which were not preincubated with 100 μM ryanodine. Control baseline $[Ca^{2+}]_i$ was 62.2 ± 11.3 nM and 76.1 ± 11.5 nM after preincubation with 100 μM ryanodine ($n = 3$). There was no statistical difference between baseline $[Ca^{2+}]_i$ with versus without 100 μM ryanodine incubation ($p = 0.06$).

Inhibition of $I_{Ca}$ by 100 nM DAMGO was measured as percentage of controls. Calcium currents treated with 100 nM DAMGO (Fig. 6*A*) were inhibited to 76.3 ± 1.8% of control currents (Fig. 7*C*). During incubation with 100 μM ryanodine (Fig. 6*B*), $I_{Ca}$ treated with 100 nM DAMGO showed no significant inhibition, being 94.6 ± 2.5% of controls ($n = 6$). There was no statistically significant difference ($p = 0.10$) between terminals in the presence of 100 μM ryanodine with and without 100 nM DAMGO.

Inactivation of $I_{Ca}$ via $Ca^{2+}$-dependent inactivation could be reflected in the time constants of inactivation of the total recorded currents. We therefore measured the time constants of

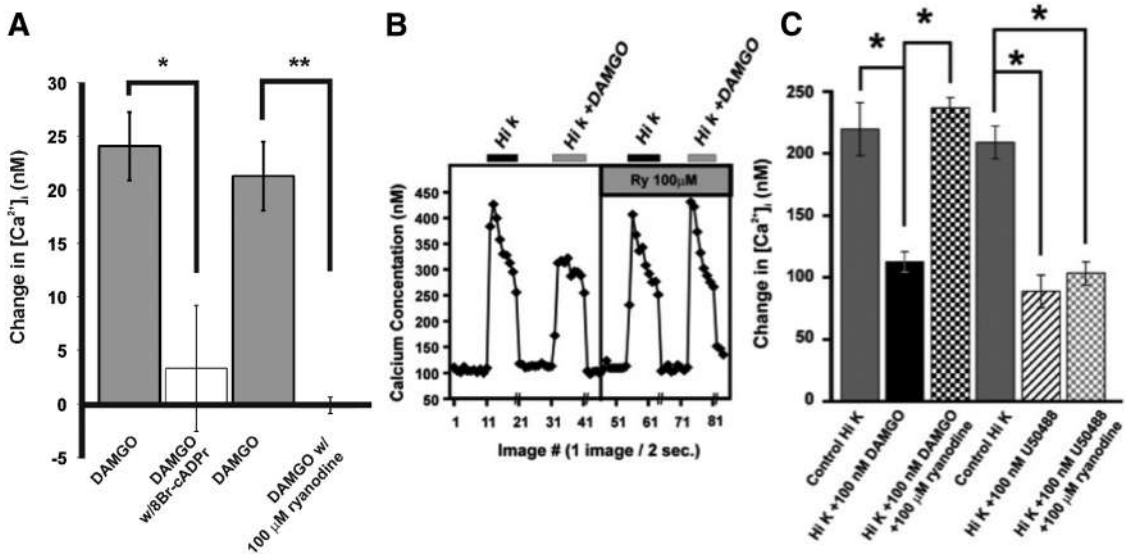


**Figure 5.** DAMGO-induced release of intraterminal calcium is reduced by either 8Br-cADPr or ryanodine, which relieves MOR- but not KOR-mediated inhibition of high-$K^+$-induced rises in $[Ca^{2+}]_i$. ***A***, $[Ca^{2+}]_i$ change from baseline in response to 100 nM DAMGO, and 100 nM DAMGO with100 nM 8Br-cADPr (as labeled); $n = 21$ terminals. Rise in basal $[Ca^{2+}]_i$ due to 100 nM DAMGO application is reduced in the presence of 100 $\mu$M ryanodine (as labeled); $n = 6$ terminals. Asterisks (**) represent statistical differences of $p = 0.0002$, and (*) represent statistical differences of $p = 0.004$. ***B***, Trace of changes in $[Ca^{2+}]_i$ in an HNS terminal with and without 100 $\mu$M ryanodine preincubation and challenged with high $K^+$ (Hi$K^+$) and high $K^+$ with 100 nM DAMGO (premixed for a simultaneous exposure). ***C***, Bar graph quantifying absolute changes in $[Ca^{2+}]_i$ in response to high $K^+$ control (without opioid or other treatment for each series; gray bars) and high $K^+$ with 100 nM DAMGO ($n = 7$) or 100 nM U50488 ($n = 5$) with and without 100 $\mu$M ryanodine plotted as absolute change in $[Ca^{2+}]_i$ (bars as labeled). Asterisk (*) represents statistically significant differences ($p = 0.001$).

inactivation of the $I_{Ca}$ (see Materials and Methods) under control (no opioid or ryanodine), 100 nM DAMGO, 100 $\mu$M ryanodine, or 100 $\mu$M ryanodine with 100 nM DAMGO conditions (Fig. 7*D*). The results were plotted as percentage of controls. The average inactivation time constant tau ($\tau$) for the control currents (±SE) was 137.0 ± 25.6 s. Calcium currents remaining in the presence of DAMGO showed slower inactivation kinetics that were 133 ± 2.6% of control. Currents with 100 nM DAMGO treatment had a $\tau = 182.14 \pm 8.7$ ms, which is different from control values ($p = 0.001$). Most interestingly, terminals treated with 100 nM DAMGO and 100 $\mu$M ryanodine had a $\tau = 131.67 \pm 12.8$ ms. In the presence of 100 $\mu$M ryanodine, these $\tau$'s were 105.4 ± 3.9% ($p = 0.77$), and, in the presence of 100 $\mu$M ryanodine and 100 nM DAMGO, they were 96.1 ± 3.7% ($p = 0.22$).

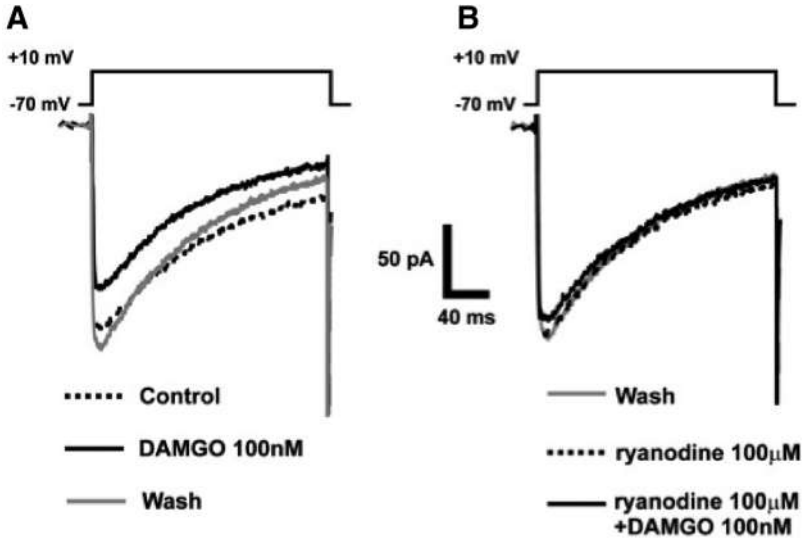


**Figure 6.** RyR antagonist relieves MOR inhibition of calcium currents. ***A***, Representative $I_{Ca}$ of an isolated HNS terminal; control currents (dashed-black), 100 nM DAMGO (black), and wash (gray). ***B***, The same isolated HNS terminal with the wash (gray) as control current followed by current trace in the presence of 100 $\mu$M ryanodine (dashed-black) and current trace in the presence of 100 $\mu$M ryanodine with 100 nM DAMGO (dashed-black).

### Effects on capacitance

Reduction of depolarization-induced neuropeptide release has been shown to be due to MOR-mediated inhibition of $I_{Ca}$ (Ortiz-Miranda et al., 2010, 2005). If MOR-mediated inhibition of $I_{Ca}$ can be blocked by 100 $\mu$M ryanodine, will it also block the MOR-mediated reduction in neuropeptide release? To address this question, we monitored changes in exocytosis/endocytosis reflected as capacitance changes in individual HNS terminals (see Materials and Methods). Changes in capacitance in perforated-patch-clamped isolated terminals in response to rectangular pulse depolarizations are inhibited by 100 nM DAMGO (Fig. 7*A*). This inhibition is almost completely reversed by 100 nM CTOP (data not shown), indicating that it is mediated by activation of the MOR. In the presence of 100 nM DAMGO, capacitance changes were 43.8 ± 8.2% of controls (Fig. 7*A*,*B*). When incubated in 100 $\mu$M ryanodine, capacitance changes were 102.9 ± 3.5% of controls. Application of 100 nM DAMGO in the presence of 100 $\mu$M ryanodine resulted in 98.2 ± 2.7% of control capacitance changes and was statistically no different from controls ($p = 0.99$) or capacitance changes in the presence of 100 mM ryanodine alone ($p = 0.16$). Time constants (two exponential fits) for each capacitance change were not significantly different between the treatments, allowing us to conclude that these effects were not on

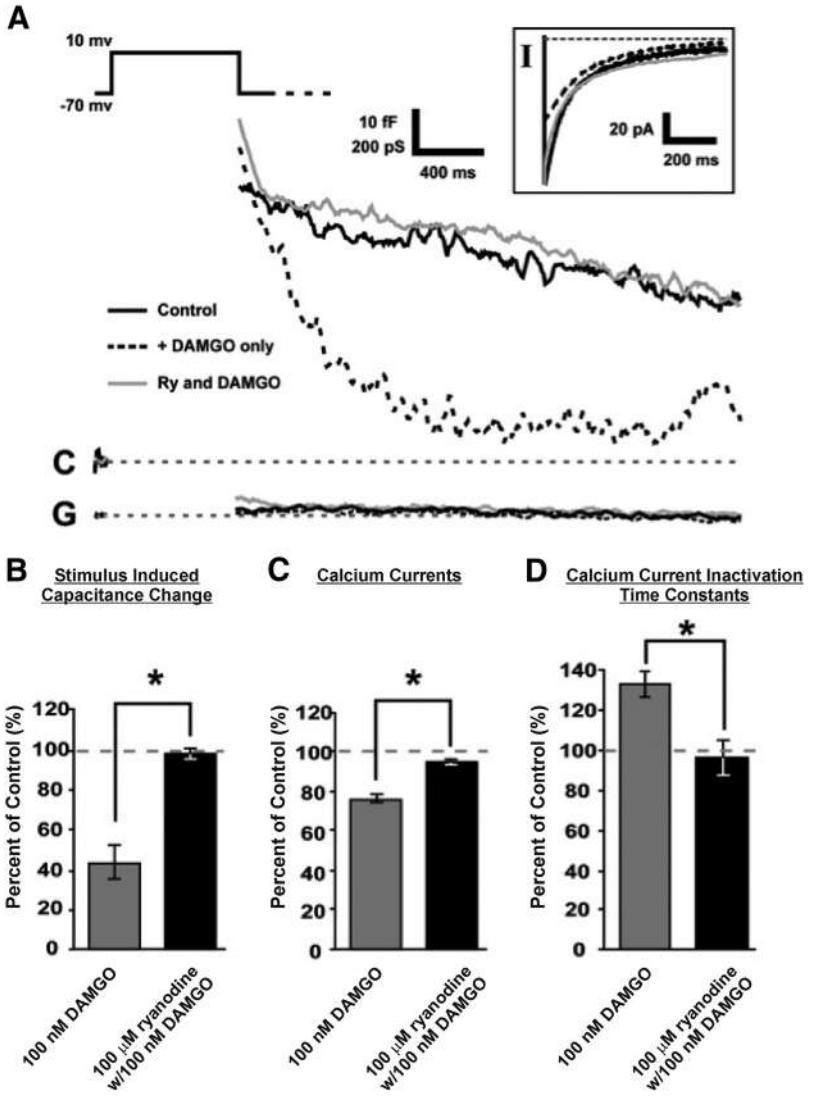


**Figure 7.** RyR antagonist relieves MOR inhibition of depolarization-induced exocytosis. ***A***, Capacitance measurements of a single terminal in the absence (black) and presence of 100 nM DAMGO (dashed-black) and of 100 $\mu$M ryanodine with 100 nM DAMGO (gray) using a square pulse of 80 mV for a duration of 750 ms. Inset shows the currents obtained from the actual stimulus (same indicators). The generalized conductance changes (G) are shown for reference. Dashed gray lines represent the zero-change baselines. Capacitance measurements in the presence of DAMGO were statistically significantly different from all other treatments ($p = 0.002$; $n = 5$). ***B***, Bar graph quantifying changes in stimulus-induced capacitance ($n = 3$) measured 1 s after cessation of stimulus in the presence of 100 nM DAMGO and 100 $\mu$M ryanodine with 100 nM DAMGO plotted as percentage of control without any drug treatment (as labeled). ***C***, Bar graph quantifying peak $I_{Ca}$ ($n = 5$) as a percentage of control peak current without drug treatment (as labeled). ***D***, Bar graph quantifying the inactivation time constants of $I_{Ca}$ ($n = 5$) as a percentage of controls without treatment (as labeled). For the decay time (inactivation), the fit was made between 5 ms after peak (to avoid multiple exponentials) and 3 ms before the end of stimulus (to avoid transient artifacts). Asterisks (*) represent statistically significant differences ($p = 0.009$).

endocytosis alone. Furthermore, we have shown previously (Ortiz-Miranda et al., 2003; Ortiz-Miranda et al., 2005) that AVP/OT release induced by high $K^+$ is inhibited by DAMGO, indicating that the net effect is inhibition of exocytosis. Therefore, antagonist concentrations of ryanodine are able to block inhibition of exocytosis by MOR activation. Nevertheless, effects on endocytosis are also possible (see Discussion).

## Discussion

The present study demonstrates that, in isolated HNS terminals, activation of the MOR elicits release of intraterminal $Ca^{2+}$ from ryanodine-sensitive stores. MOR-mediated inhibition of $I_{Ca}$ and of high-$K^+$-induced rises in $[Ca^{2+}]_i$ can be blocked by antagonist concentrations of ryanodine and reduced by inhibition of the cADPr pathway. Changes in the inactivation kinetics of $I_{Ca}$ in the presence of MOR agonists suggests that release of intraterminal $Ca^{2+}$ could be responsible for $Ca^{2+}$-dependent inactivation of $I_{Ca}$. However, because stores cannot be depleted and ryanodine receptor (RyR) KO animals are not viable (De Crescenzo et al., 2012), it is not possible to prove this. Nevertheless, showing that BAPTA, ryanodine and 8Br-cADPr are all capable of blocking DAMGO's effects is strong evidence in support of the role of intraterminal $Ca^{2+}$ stores in mediating MOR inhibition.

Furthermore, MOR-mediated inhibition of capacitance in individual terminals can also be blocked by antagonist concentrations of ryanodine. These data support the hypothesis (Fig. 8) that MOR activation leads to the release of $Ca^{2+}$ from ryanodine-sensitive stores via activation of the cADPr pathway, possibly leading to $Ca^{2+}$-dependent inactivation of $I_{Ca}$ and subsequent inhibition of depolarization-secretion coupling (DSC).

### cADPr pathway and ryanodine-sensitive stores in HNS terminals

Oxytocin secretion is most sensitive to MOR-mediated inhibition (Wright and Clarke, 1984; Bicknell et al., 1985; Zhao et al., 1988; Leng et al., 1992; Russell et al., 1995; Ortiz-Miranda et al., 2005). Vasopressin release, although responsive to MOR-mediated inhibition, is less sensitive to MOR agonists (Ortiz-Miranda et al., 2003). Interestingly, in HNS terminals, blocking cADPr signaling was shown to attenuate high-$K^+$ induced rises in $[Ca^{2+}]_i$, but only inhibited OT release from isolated terminals (Higashida et al., 2007; Jin et al., 2007). This strongly suggests that the cADPr pathway is both present in OT terminals and linked to neuropeptide release and thus may be responsible for OT-terminal-heightened sensitivity to MOR-mediated inhibition (Fig. 8).

CD38 is a catalyst for the formation of cADPr and nicotinic acid adenine dinucleotide phosphate by ADP-ribosyl cyclase from $NAD^+$ and NAD phosphate (Lee, 1998). Both are known to release $Ca^{2+}$ from intracellular ryanodine-sensitive pools as part of a second messenger-signaling pathway. In studies monitoring depolarization-induced OT secretion in murine NH terminals (Jin et al., 2007), CD38 $^{-/-}$ mice showed severe and selective impairment of OT release. Currently, this contribution of the cADPr pathway to depolarization-induced responses appears to be in conflict with our results showing the cADPr pathway mediating $I_{Ca}$ inhibition triggered by activation of the MOR (Fig. 8). Although it is clear that the

cADPr pathway in HNS terminals can modulate the depolarization-induced response, our results suggest that it may do so differentially depending on the compartments/circumstances in which the pathway is activated. For example, in our model (Fig. 8), MOR activation of the cADPr pathway releases $Ca^{2+}$ from RyRs and, via PK/PP, leads to inactivation of nearby, closed VGCCs. Upon depolarization, these VGCCs would not be available for activation, leading to less neuropeptide release. Direct activation of a specific pool of intraterminal calcium stores during depolarization-induced responses, however, via the cADPr pathway could directly target specific release sites, resulting in potentiation of the response. We have previously demonstrated $Ca^{2+}$ sparks or "syntillas" in murine HNS terminals that are both ryanodine and voltage sensitive (De Crescenzo et al., 2004, 2006). Syntillas result from the activation of both type-1 and type-2 RyRs. Presumably, the type-1 RyR confers the voltage sensitivity via direct interaction with dihydropyridine receptors (De Crescenzo et al., 2006), as documented in skeletal muscle (Schneider and Chandler, 1973; Inui et al., 1987). The cADPr pathway may assist in amplifying this direct effect in HNS terminals during DSC. Inhibition of voltage-dependent release of calcium from ryanodine-sensitive stores may account for the inhibition of both the depolarization-induced rise in $[Ca^{2+}]_i$ and oxytocin release observed in the presence of 200 $\mu$M ryanodine, as described previously (Jin et al., 2007). However, Jin et al. (2007) showed no effects on AVP release, which would be consistent with our lack of capacitance changes in the presence of 100 $\mu$M ryanodine alone (Fig. 7*A*). Activation of the cADPr-pathway via the MOR could result in a release of $[Ca^{2+}]_i$ from a different subset of ryanodine receptors (see model in Fig. 8) that both temporally and spatially result in calcium-induced inhibition of $I_{Ca}$ and subsequent inhibition of neuropeptide release. The relative ratio of these effects would determine the net impact on DSC (see model in Fig. 8 describing the transduction mechanisms thought to underlie the MOR and KOR effects seen in this system in relation to oxytocin release).

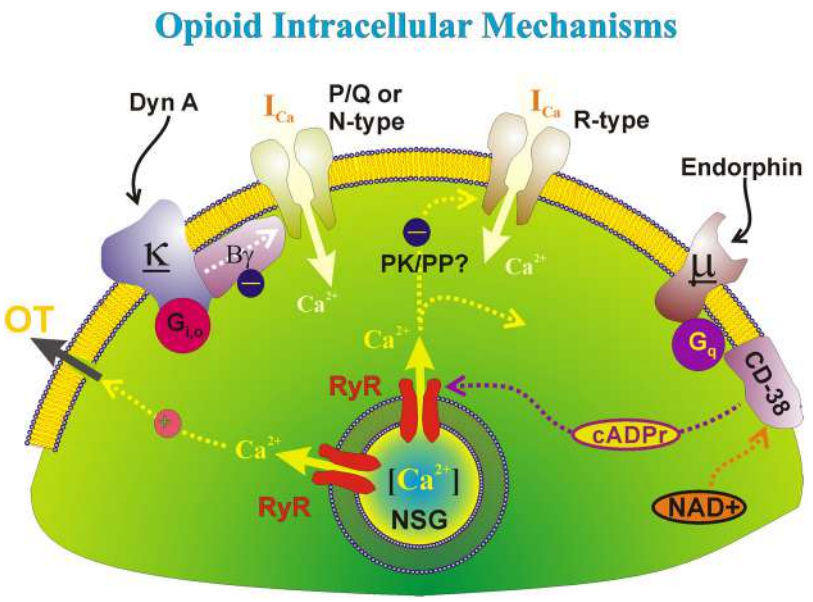


**Figure 8.** Model for opioid modulation of calcium currents. Activation of the MOR initiates cADPr signaling, presumably via $G_q$ activation of ADP-rybosyl cyclase/CD38 complex catalyzing the conversion of $NAD^+$ into cADPr. Cyclic-ADPr subsequently leads to activation of RyRs on neurosecretory granules (NSGs) in the terminals. Release of the diffusible second messenger $Ca^{2+}$ from ryanodine-sensitive stores subsequently results in $Ca^{2+}$-dependent inactivation of closed VGCCs possibly via protein kinases (PKs) and/or protein phosphatases (PPs). In contrast, activation of the KOR initiates $G_{i,o}$ $\alpha$-protein dissociation from $G_\beta\gamma$ subunits. $G_\beta\gamma$ mediates membrane-delimited voltage-dependent inhibition of $I_{Ca}$ via direct interaction with the closed or resting channel. Inhibition (−) of $I_{Ca}$ would lead to decreased release of OT. In contrast, $Ca^{2+}$-induced $Ca^{2+}$-release from RyR stores would stimulate (+) OT secretion (Jin et al., 2007).

There are some other important considerations that must also be addressed to interpret our results. First, the concentration of 8Br-cADPr used in our study was 100 nM, in contrast to the 100 $\mu$M used in previous studies (Jin et al., 2007). Preliminary calcium imaging of rat isolated HNS terminals shows a significant rise in basal $[Ca^{2+}]_i$ in the presence of higher (100–300 $\mu$M) concentrations of 8Br-cADPr (data not shown), which does not occur at the 100 nM concentration. This could theoretically have the same effects as those seen for MOR activation, leading to subsequent calcium-dependent inactivation of $I_{Ca}$ and attenuated neuropeptide release. Therefore, the presence of 8Br-cADPr at higher concentrations would, by itself, saturate the calcium-induced inhibitory response in the HNS rat preparation.

Furthermore, $IP_3$ receptor effects have been observed in NH terminals (Cazalis et al., 1987) and, because they often work in concert with RyRs, there could also be such a role for $IP_3$ receptors.

### MOR effects on calcium currents and subsequent release

In cardiac tissue, changes in $[Ca^{2+}]_i$ can lead to inactivation of VGCCs (Morad, 1995). Calcium-dependent inactivation of VGCCs in HNS terminals has been demonstrated previously (Branchaw et al., 1997; Wang et al., 1999). Similarly, $\mu$-opioid inhibition of $I_{Ca}$ results in a decreased rate of inactivation of the remaining $I_{Ca}$ during a depolarizing stimulation pulse (Fig. 7*D*). Presumably, the fraction of $I_{Ca}$ remaining after calcium-dependent inactivation represents currents shielded from the effects of intraterminal $Ca^{2+}$. It is also possible that a $Ca^{2+}$-dependent process (e.g., protein kinase or phosphatase; Ortiz-Miranda et al., 2010) is involved (see model legend in Fig. 8). Although the mechanism underlying this phenomenon is unknown, VGCCs in terminals are unique in other ways. The *N*-type $Ca^{2+}$ channels in the NH (Lemos and Nowycky, 1989; Wang et al., 1993) have lower single-schannel conductance and more rapid inactivation kinetics than those observed for conventional somatic channels (Bean, 1989; Wang et al., 1993). In our model, release of calcium from ryanodine-sensitive stores may lead to calcium-dependent inactivation of VGCCs and a reduced $I_{Ca}$. The remaining $I_{Ca}$ has slower inactivation kinetics, possibly indicating that they are only exhibiting $Ca^{2+}$-independent inactivation (Fig. 7*D*). This reduction in $I_{Ca}$ would lead to decreased exocytosis (Fig. 7*A*) of neuropeptides from the terminals.

We cannot say unequivocally that exocytosis is the sole contributor to the effects of MOR modulation of $I_{Ca}$ on release dynamics that we report here. It is possible that our observations include effects on endocytosis or on exo-endocytosis (e.g., increases in "kiss and run"). However, we believe the exocytotic

component is a major contributor to the modulation we observe. Among other evidence, the most compelling to suggest this is the fact that when we blocked endocytosis using $Ba^{2+}$ instead of $Ca^{2+}$ (data not shown), DAMGO still inhibited the elicited capacitance changes.

## Conclusions

Diffusible second messenger amplification of MOR signaling via cADPr-mediated release of $Ca^{2+}$ from a ryanodine-sensitive stores seems well suited for regulating OT release during the relatively long period of gestation. It is during this time that endogenous MOR-mediated inhibition of release accumulates OT, but is then interrupted during parturition and subsequent lactation (Russell et al., 1989; Douglas et al., 1995; Russell et al., 1995; Ortiz-Miranda et al., 2003). Interestingly, opioid-receptor-induced $Ca^{2+}$ mobilization has also been observed in both murine astrocytes (Hauser et al., 1996) and isolated rat ventricular myocytes (Tai et al., 1992). Intraterminal calcium release and its associated $Ca^{2+}$ microdomains likely have a wide range of possible targets and subsequent effects on depolarization-secretion coupling (Berridge, 2006; Oheim et al., 2006). Therefore, ryanodine-sensitive stores in HNS terminals may prove to be bimodal regulators of release depending on the physiological circumstances. Given the emerging role of ryanodine-sensitive stores and the cADPr signaling pathway in the CNS, our results represent an important contribution to our understanding of their physiological role in presynaptic terminals during DSC.

## References


Bean BP (1989) Classes of calcium channels in vertebrate cells. Annu Rev Physiol 51:367–384. CrossRef Medline

Berridge MJ (2006) Calcium microdomains: organization and function. Cell Calcium 40:405–412. CrossRef Medline

Bicknell RJ, Chapman C, Leng G (1985) Effects of opioid agonists and antagonists on oxytocin and vasopressin release in vitro. Neuroendocrinology 41:142–148. CrossRef Medline

Branchaw JL, Banks MI, Jackson MB (1997) $Ca^{2+}$- and voltage-dependent inactivation of $Ca^{2+}$ channels in nerve terminals of the neurohypophysis. J Neurosci 17:5772–5781. Medline

Brethes D, Dayanithi G, Letellier L, Nordmann JJ (1987) Depolarization-induced $Ca^{2+}$ increase in isolated neurosecretory nerve terminals measured with fura-2. Proc Natl Acad Sci U S A 84:1439–1443. CrossRef Medline

Brown CH, Bourque CW (2004) Autocrine feedback inhibition of plateau potentials terminates phasic bursts in magnocellular neurosecretory cells of the rat supraoptic nucleus. J Physiol 557:949–960. CrossRef Medline

Brown CH, Ludwig M, Leng G (2004) Temporal dissociation of the feedback effects of dendritically co-released peptides on rhythmogenesis in vasopressin cells. Neuroscience 124:105–111. CrossRef Medline

Brown CH, Leng G, Ludwig M, Bourque CW (2006) Endogenous activation of supraoptic nucleus kappa-opioid receptors terminates spontaneous phasic bursts in rat magnocellular neurosecretory cells. J Neurophysiol 95:3235–3244. CrossRef Medline

Cazalis M, Dayanithi G, Nordmann JJ (1987) Requirements for hormone release from permeabilized nerve endings isolated from the rat neurohypophysis. J Physiol 390:71–91. Medline

Chen X, Marrero HG, Murphy R, Lin YJ, Freedman JE (2000) Altered gating of opiate receptor-modulated K+ channels on amygdala neurons of morphine-dependent rats. Proc Natl Acad Sci U S A 97:14692–14696. CrossRef Medline

Connor M, Christie MD (1999) Opioid receptor signalling mechanisms. Clin Exp Pharmacol Physiol 26:493–499. CrossRef Medline

Coronado R, Morrissette J, Sukhareva M, Vaughan DM (1994) Structure and function of ryanodine receptors. Am J Physiol 266:C1485–1504. Medline

De Crescenzo V, ZhuGe R, Velázquez-Marrero C, Lifshitz LM, Custer E, Carmichael J, Lai FA, Tuft RA, Fogarty KE, Lemos JR, Walsh JV Jr (2004) $Ca^{2+}$ syntillas, miniature $Ca^{2+}$ release events in terminals of hypothalamic neurons, are increased in frequency by depolarization in the absence of $Ca^{2+}$ influx. J Neurosci 24:1226–1235. CrossRef Medline

De Crescenzo V, Fogarty KE, Zhuge R, Tuft RA, Lifshitz LM, Carmichael J, Bellvé KD, Baker SP, Zissimopoulos S, Lai FA, Lemos JR, Walsh JV Jr (2006) Dihydropyridine receptors and type 1 ryanodine receptors constitute the molecular machinery for voltage-induced $Ca^{2+}$ release in nerve terminals. J Neurosci 26:7565–7574. CrossRef Medline

De Crescenzo V, Fogarty KE, Lefkowitz JJ, Bellve KD, Zvaritch E, MacLennan DH, Walsh JV Jr (2012) Type 1 ryanodine receptor knock-in mutation causing central core disease of skeletal muscle also displays a neuronal phenotype. Proc Natl Acad Sci U S A 109:610–615. CrossRef Medline

Douglas AJ, Neumann I, Meeren HK, Leng G, Johnstone LE, Munro G, Russell JA (1995) Central endogenous opioid inhibition of supraoptic oxytocin neurons in pregnant rats. J Neurosci 15:5049–5057. Medline

Ehrlich BE, Kaftan E, Bezprozvannaya S, Bezprozvanny I (1994) The pharmacology of intracellular Ca(2+)-release channels. Trends Pharmacol Sci 15:145–149. CrossRef Medline

Galione A (1994) Cyclic ADP-ribose, the ADP-ribosyl cyclase pathway and calcium signalling. Mol Cell Endocrinol 98:125–131. CrossRef Medline

Gillis KD (1995) Techniques for membrane capacitance measurements. In Single-Channel Recording. New York, Plenum

Grynkiewicz G, Poenie M, Tsien RY (1985) A new generation of $Ca^{2+}$ indicators with greatly improved fluorescence properties. J Biol Chem 260:3440–3450. Medline

Hauser KF, Stiene-Martin A, Mattson MP, Elde RP, Ryan SE, Godleske CC (1996) mu-Opioid receptor-induced $Ca^{2+}$ mobilization and astroglial development: morphine inhibits DNA synthesis and stimulates cellular hypertrophy through a Ca(2+)-dependent mechanism. Brain Res 720:191–203. CrossRef Medline

Higashida H, Salmina AB, Olovyannikova RY, Hashii M, Yokoyama S, Koizumi K, Jin D, Liu HX, Lopatina O, Amina S, Islam MS, Huang JJ, Noda M (2007) Cyclic ADP-ribose as a universal calcium signal molecule in the nervous system. Neurochem Int 51:192–199. CrossRef Medline

Inui M, Saito A, Fleischer S (1987) Purification of the ryanodine receptor and identity with feet structures of junctional terminal cisternae of sarcoplasmic reticulum from fast skeletal muscle. J Biol Chem 262:1740–1747. Medline

Jin D, Liu HX, Hirai H, Torashima T, Nagai T, Lopatina O, Shnayder NA, Yamada K, Noda M, Seike T, Fujita K, Takasawa S, Yokoyama S, Koizumi K, Shiraishi Y, Tanaka S, Hashii M, Yoshihara T, Higashida K, Islam MS, et al. (2007) CD38 is critical for social behaviour by regulating oxytocin secretion. Nature 446:41–45. CrossRef Medline

Kaneko S, Akaike A, Satoh M (1998) Differential regulation of N- and Q-type $Ca^{2+}$ channels by cyclic nucleotides and G-proteins. Life Sci 62:1543–1547. Medline

Kato M, Chapman C, Bicknell RJ (1992) Activation of kappa-opioid receptors inhibits depolarisation-evoked exocytosis but not the rise in intracellular $Ca^{2+}$ in secretory nerve terminals of the neurohypophysis. Brain Res 574:138–146. CrossRef Medline

Knott TK, Velázquez-Marrero C, Lemos JR (2005) ATP elicits inward currents in isolated vasopressinergic neurohypophysial terminals via P2X2 and P2X3 receptors. Pflugers Arch 450:381–389. CrossRef Medline

Knott TK, Marrero HG, Fenton RA, Custer EE, Dobson JG Jr, Lemos JR (2007) Endogenous adenosine inhibits CNS terminal Ca(2+) currents and exocytosis. J Cell Physiol 210:309–314. CrossRef Medline

Lee HC (1998) Calcium signaling by cyclic ADP-ribose and NAADP–a decade of exploration. Cell Biochem Biophys 28:1–17. CrossRef Medline

Lemos JR, Nowycky MC (1989) Two types of calcium channels coexist in peptide-releasing vertebrate nerve terminals. Neuron 2:1419–1426. CrossRef Medline

Lemos JR, Nordmann JJ, Cooke IM, Stuenkel EL (1986) Single channels and ionic currents in peptidergic nerve terminals. Nature 319:410–412. CrossRef Medline

Leng G, Dyball RE, Way SA (1992) Naloxone potentiates the release of oxytocin induced by systemic administration of cholecystokinin without enhancing the electrical activity of supraoptic oxytocin neurones. Exp Brain Res 88:321–325. CrossRef Medline

Lindau M, Neher E (1988) Patch-clamp techniques for time-resolved capacitance measurements in single cells. Pflugers Arch 411:137–146. CrossRef Medline

Morad M (1995) Signaling of $Ca^{2+}$ release and contraction in cardiac myocytes. Adv Exp Med Biol 382:89–96. CrossRef Medline

Morita K, Kitayama S, Dohi T (2002) Physiological role of cyclic ADP-ribose as a novel endogenous agonist of ryanodine receptor in adrenal chromaffin cells [article in Japanese]. Nippon Yakurigaku Zasshi 120: 96P–98P. Medline

Neher E, Marty A (1982) Discrete changes of cell membrane capacitance observed under conditions of enhanced secretion in bovine adrenal chromaffin cells. Proc Natl Acad Sci U S A 79:6712–6716. CrossRef Medline

Nordmann JJ, Dayanithi G, Lemos JR (1987) Isolated neurosecretory nerve endings as a tool for studying the mechanism of stimulus-secretion coupling. Biosci Rep 7:411–426. CrossRef Medline

Oheim M, Kirchhoff F, Stühmer W (2006) Calcium microdomains in regulated exocytosis. Cell Calcium 40:423–439. CrossRef Medline

Ortiz-Miranda SI, Dayanithi G, Coccia V, Custer EE, Alphandery S, Mazuc E, Treistman S, Lemos JR (2003) mu-Opioid receptor modulates peptide release from rat neurohypophysial terminals by inhibiting Ca(2+) influx. J Neuroendocrinol 15:888–894. CrossRef Medline

Ortiz-Miranda SI, Dayanithi G, Velázquez-Marrero C, Custer EE, Treistman SN, Lemos JR (2010) Differential modulation of N-type calcium channels by micro-opioid receptors in oxytocinergic versus vasopressinergic neurohypophysial terminals. J Cell Physiol 225:276–288. CrossRef Medline

Ortiz-Miranda S, Dayanithi G, Custer E, Treistman SN, Lemos JR (2005) Micro-opioid receptor preferentially inhibits oxytocin release from neurohypophysial terminals by blocking R-type $Ca^{2+}$ channels. J Neuroendocrinol 17:583–590. CrossRef Medline

Roper P, Callaway J, Armstrong W (2004) Burst initiation and termination in phasic vasopressin cells of the rat supraoptic nucleus: a combined mathematical, electrical, and calcium fluorescence study. J Neurosci 24: 4818–4831. CrossRef Medline

Rusin KI, Giovannucci DR, Stuenkel EL, Moises HC (1997) k-opioid receptor activation modulates $Ca^{2+}$ currents and secretion in isolated neuroendocrine nerve terminals. J Neurosci 17:6565–6574. Medline

Russell JA, Gosden RG, Humphreys EM, Cutting R, Fitzsimons N, Johnston V, Liddle S, Scott S, Stirland JA (1989) Interruption of parturition in rats by morphine: a result of inhibition of oxytocin secretion. J Endocrinol 121:521–536. CrossRef Medline

Russell JA, Coombes JE, Leng G, Bicknell RJ (1993) Morphine tolerance and inhibition of oxytocin secretion by kappa-opioids acting on the rat neurohypophysis. J Physiol 469:365–386. Medline

Russell JA, Leng G, Bicknell RJ (1995) Opioid tolerance and dependence in the magnocellular oxytocin system: a physiological mechanism? Exp Physiol 80:307–340. Medline

Russell JA, Leng G, Douglas AJ (2003) The magnocellular oxytocin system, the fount of maternity: adaptations in pregnancy. Front Neuroendocrinol 24:27–61. CrossRef Medline

Sabatier N, Leng G (2007) Bistability with hysteresis in the activity of vasopressin cells. J Neuroendocrinol 19:95–101. CrossRef Medline

Samways DS, Henderson G (2006) Opioid elevation of intracellular free calcium: possible mechanisms and physiological relevance. Cell Signal 18:151–161. CrossRef Medline

Schneider MF, Chandler WK (1973) Voltage dependent charge movement of skeletal muscle: a possible step in excitation-contraction coupling. Nature 242:244–246. CrossRef Medline

Sitsapesan R, McGarry SJ, Williams AJ (1995) Cyclic ADP-ribose, the ryanodine receptor and $Ca^{2+}$ release. Trends Pharmacol Sci 16:386–391. CrossRef Medline

Soldo BL, Moises HC (1998) mu-Opioid receptor activation inhibits N- and P-type $Ca^{2+}$ channel currents in magnocellular neurones of the rat supraoptic nucleus. J Physiol 513:787–804. CrossRef Medline

Stuenkel EL, Nordmann JJ (1993) Intracellular calcium and vasopressin release of rat isolated neurohypophysial nerve endings. J Physiol 468:335–355. Medline

Sumner BE, Coombes JE, Pumford KM, Russell JA (1990) Opioid receptor subtypes in the supraoptic nucleus and posterior pituitary gland of morphine-tolerant rats. Neuroscience 37:635–645. CrossRef Medline

Tai KK, Bian CF, Wong TM (1992) kappa-Opioid receptor stimulation increases intracellular free calcium in isolated rat ventricular myocytes. Life Sci 51:909–913. CrossRef Medline

Velázquez-Marrero CM, Marrero HG, Lemos JR (2010) Voltage-dependent kappa-opioid modulation of action potential waveform-elicited calcium currents in neurohypophysial terminals. J Cell Physiol 225:223–232. CrossRef Medline

Wang G, Dayanithi G, Newcomb R, Lemos JR (1999) An R-type Ca(2+) current in neurohypophysial terminals preferentially regulates oxytocin secretion. J Neurosci 19:9235–9241. Medline

Wang X, Treistman SN, Lemos JR (1993) Single channel recordings of Nt- and L-type $Ca^{2+}$ currents in rat neurohypophysial terminals. J Neurophysiol 70:1617–1628. Medline

Wilding TJ, Womack MD, McCleskey EW (1995) Fast, local signal transduction between the mu opioid receptor and $Ca^{2+}$ channels. J Neurosci 15:4124–4132. Medline

Wright DM, Clarke G (1984) Inhibition of oxytocin secretion by mu and delta receptor selective enkephalin analogues. Neuropeptides 5:273–276. CrossRef Medline

Zhao BG, Chapman C, Bicknell RJ (1988) Opioid-noradrenergic interactions in the neurohypophysis. I. Differential opioid receptor regulation of oxytocin, vasopressin, and noradrenaline release. Neuroendocrinology 48:16–24. CrossRef Medline